

Multi-frequency scatterometer measurements on water surfaces agitated by artificial and natural rain

N. BRAUN* and M. GADE

Institut für Meereskunde, Universität Hamburg, Bundesstraße 53, 20146 Hamburg, Germany

(Received 15 July 2004; in final form 30 June 2005)

Images of rain events over the ocean acquired by a multi-frequency/multi-polarization Synthetic Aperture Radar (SAR) show different radar contrasts at different frequencies and polarizations. In order to better understand these effects, field and laboratory experiments were performed at different rain rates and wind speeds with scatterometers working at different radar frequencies, polarizations, and incidence angles. Our results show that the dominant scattering mechanism on a rain-roughened water surface, observed at VV polarization, at all incidence angles is Bragg scattering from ring waves. At HH polarization the radar backscatter is caused by both ring waves and non-propagating splash products, with the dominating effect depending on incidence angle. The reduction and enhancement of the surface roughness by ring waves and sub-surface phenomena, respectively, result in a transition wavenumber between reduction of the radar backscattering and its enhancement of about 100 rad m^{-1} . We assume that this transition wavenumber depends on the drop-size distribution of the rain. Taking into consideration the different dependencies of the radar backscatter at different frequencies and polarizations on rain rate, we suggest a method to estimate rain rates by calculating the ratio of the radar cross-sections at L band, VV polarization and at C band, HV polarization. Provided an availability of SAR data at the respective frequency–polarization combinations, this method allows for investigating the nature of small-scale (convective) rain events over the ocean.

1. Introduction

Estimating rain rates of rain events over the sea is important for determining fluxes of momentum, water, heat, and gas at the air–water interface, as well as the production of sea salt aerosols. Synthetic Aperture Radar (SAR) images of strong rain events over the ocean surface show different image contrasts that are related to the action of combined wind and rain effects on the water surface, as first observed by Fu and Holt (1982) and analysed by Atlas (1994). These image contrasts depend on radar frequency and polarization (Melsheimer *et al.* 1998). Under the action of strong rain the small-scale roughness of the sea surface is changed, which in turn affects its radar backscattering properties. If the mechanisms of the radar backscattering from rain-roughened water surfaces are understood, information

*Corresponding author. Present address: Institut für Küstenforschung, GKSS-Forschungszentrum, Max-Planck-Straße, 21502 Geesthacht, Germany. Email: nicole.braun@gkss.de

on the local distribution and intensity of rain over the ocean surface can be inferred from multi-frequency/multi-polarization SAR images.

Former laboratory investigations at steep incidence angles show that at VV polarization ring waves are the main scatterers at Ku band (Bliven *et al.* 1993) and X band (Braun *et al.* 2002). Braun *et al.* (2002) have shown by laboratory investigations that different scattering mechanisms are responsible for a strong increase of the HV polarization backscatter in the presence of heavy rain.

In order to gain more knowledge of the radar backscattering from rain-roughened water surfaces, field experiments were performed with a multi-frequency/multi-polarization microwave scatterometer under different wind and rain conditions. In addition, laboratory experiments were conducted to investigate the incidence-angle dependency of the radar backscatter at VV and HH polarization. The results of these investigations allow new insights into the transition domain from reduction to enhancement of the surface roughness by rain. Based on our results, a new method for estimating rain rates of small-scale rain events over the ocean will be suggested.

2. Experimental set-up

2.1 Field measurements

The field measurements were performed with a multi-frequency/multi-polarization microwave scatterometer mounted on a tower located directly at the mouth of the river Elbe in the German Bight of the North Sea (see figure 1).

The measurements were performed quasi-simultaneously at microwave frequencies of 2.4 GHz (S band), 5.3 GHz (C band) and 10 GHz (X band), at VV, HV and HH polarization. By tilting the antenna in steps of 5° , incidence angles between 30° and 50° were covered.

The minimum size of the radar footprint was $0.7\text{ m} \times 0.6\text{ m}$ (X band, 30°) and the maximum size was $6.1\text{ m} \times 3.9\text{ m}$ (S band, 50°) (see table 1). Data were acquired at a sample rate of 10 KHz per channel. Figure 2 shows a sketch of the set-up and geometry of antenna height and footprint of the scatterometer. A more detailed description of the microwave system was given by Wismann (1994).

Accompanying time series of wind speed, wind direction, and rain rate were acquired by sensors mounted on the tower's roof. In order to investigate the influence of rain on the radar backscatter we selected pairs of measurements that were performed with and without rain, but under similar residual conditions (incidence angle, wind speed and direction).

2.2 Laboratory measurements

The laboratory measurements were performed at the wind-wave tank of the University of Hamburg (Hühnerfuß *et al.* 1976) with a 9.8 GHz (X band) microwave scatterometer. The incidence angles were 29° , 40° , 55° and 78° , the radar polarizations were HH, VV and HV (not at 78°). The area agitated by artificial rain was 2.3 m long and 1 m wide. The scatterometer antennas were mounted facing upwind, and the radar footprint was at a fetch of 14.5 m, well inside the area agitated by rain (see figure 3). A more detailed description of the experimental set-up can be found in Braun *et al.* (2002). The measurements were performed for combinations of wind speeds from 2 to 10 m s^{-1} , and rain rates of 50 and 100 mm h^{-1} . A fixed raindrop size of 2.9 mm diameter was used. The parameters of the dataset are given in table 2.

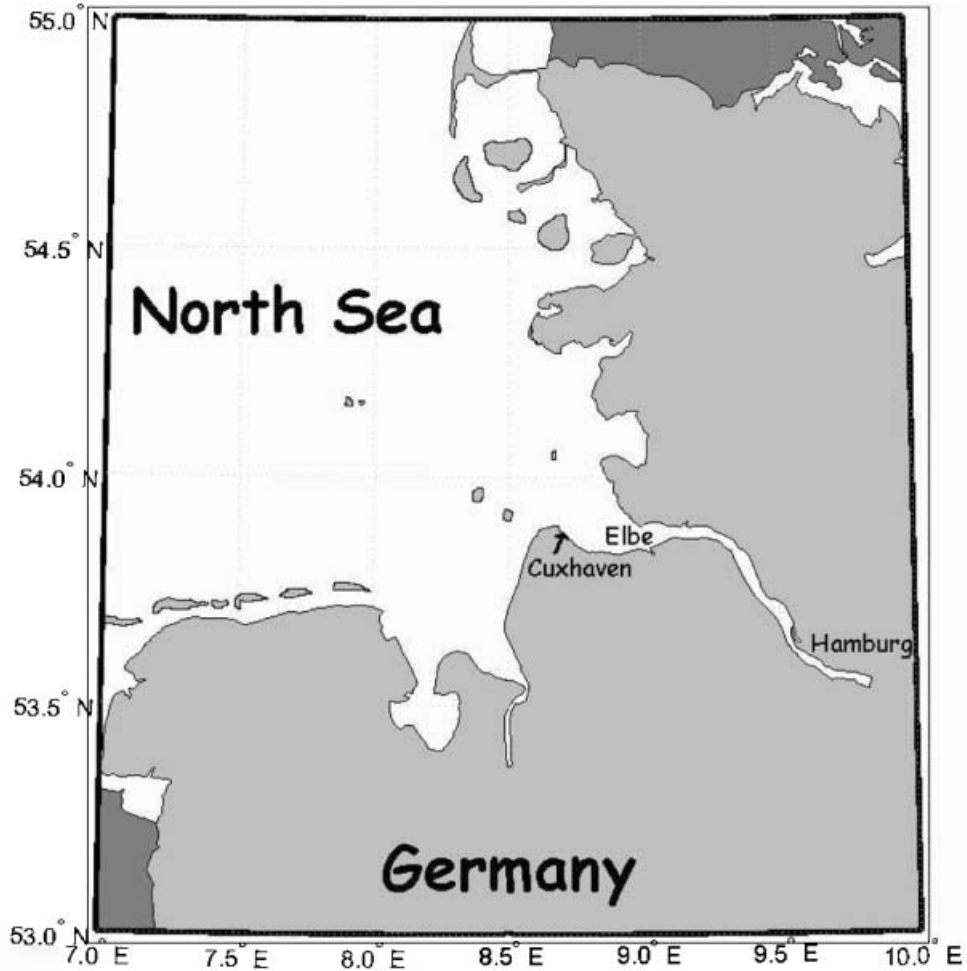


Figure 1. The test site of the field measurements at Cuxhaven port at the mouth of the river Elbe in the German Bight.

Table 1. Geometrical parameters of the deployed antenna system. The minimum and maximum footprint sizes were calculated assuming minimum and maximum antenna heights and incidence angles.

	Antenna geometry		
	S band 2.4 GHz	C band 5.3 GHz	X band 10.0 GHz
Antenna beam width (two-way)	5.6°	2.5°	1.4°
Minimum footprint size (22.5 m, 30°)	2.9 m × 2.5 m	1.3 m × 1.1 m	0.7 m × 0.6 m
Maximum footprint size (25.5 m, 50°)	6.1 m × 3.9 m	2.7 m × 1.7 m	1.5 m × 1.0 m

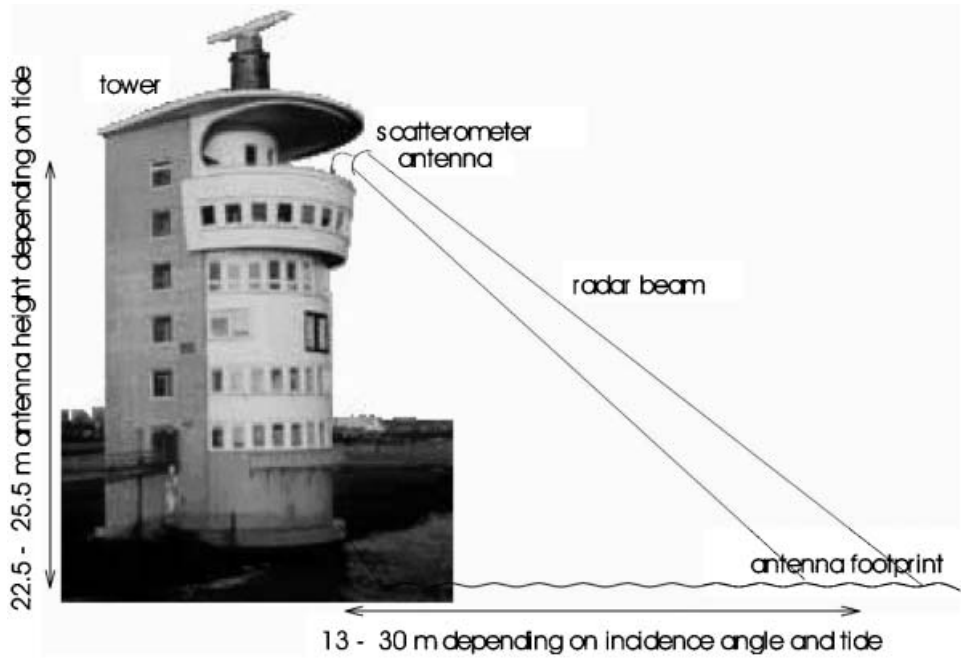


Figure 2. Sketch of the experimental set-up of the multi-frequency/multi-polarization microwave scatterometer.

For the field and laboratory measurements radar Doppler spectra were calculated from the time series of the backscattered radar signal of 32 and 140 s length, respectively.

Faulty data were rejected and the radar Doppler spectra were corrected for noise effects of the hardware. Integrating over all values exceeding $1/4$ (i.e. -6 dB) of the spectral maximum the relative radar cross-sections were calculated. Since only relative changes in the radar backscatter were investigated within this study, we have refrained from absolutely calibrating the scatterometer systems.

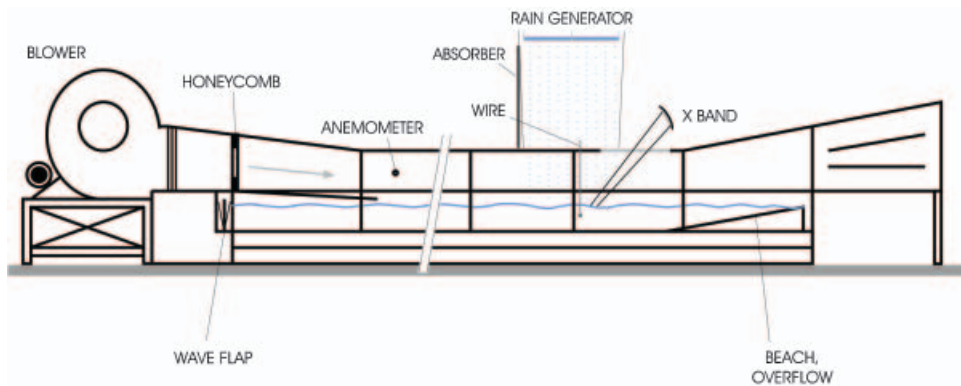


Figure 3. Schematic side view of the wind-wave tank with the rain generator and X band radar.

Table 2. Dataset of the wind-wave tank measurements of the wave amplitude and radar backscattering.

Incidence angle (°)	Dataset of the wind-wave tank measurements		
	Radar polarization (°)	Wind speed (m s ⁻¹)	Rain rate (mm h ⁻¹)
29	VV, HH and HV	0,2,3,4,...,10	0, 50 and 100
40	VV, HH and HV	0,2,3,4,...,10	0, 50 and 100
55	VV, HH and HV	0,2,3,4,...,10	0, 50 and 100
78	VV and HH	0,2,3,4,...,10	0 and 40

3. Results and discussion

3.1 Co-polarization, field measurements

Figure 4 shows radar Doppler spectra obtained during field measurements at S, C and X bands, VV polarization at an incidence angle of 35°, before and during a rain event. This rain event was a strong rain shower with a maximum rain rate of 35 mm h⁻¹. Without rain (left column), one single Doppler maximum was measured at all polarizations, which results from the radar backscattering at the wind-roughened water surface (wind speed: 7.5 m s⁻¹, azimuth angle, i.e. the angle between the antenna facing direction and wind direction: 255°). The spike at +20 Hz observed at C band (middle left panel) is likely to be due to electrical noise and is therefore not considered in our analyses. During the rain event (right column; wind speed: 6.5 m s⁻¹, azimuth angle: 275°) the shape of the spectra changed dramatically: while at X band the power spectral density (PSD) was enhanced and a broad maximum developed, at C and S bands two maxima were measured. The radar Doppler spectra at HH polarization look similar to those at VV polarization (not shown herein). Due to the river current the two maxima are shifted towards lower Doppler frequencies. Neglecting this effect, the Doppler frequencies of these maxima are ±3.8 Hz (S band) and ±6.4 Hz (C band) and thus coincide with the respective resonant Bragg frequencies. Thus, our results confirm that under natural conditions at steep incidence angles at co-polarization rain ring waves cause the radar backscattering from a water surface during strong rain events.

3.2 Co-polarization, laboratory measurements

To investigate the incidence angle dependency at co-polarization, laboratory investigations were performed. Figure 5 shows the radar Doppler spectra obtained in laboratory measurements at X band VV and HH polarization, without wind. At incidence angles of 29°, 40° and 55° the rain rate was 50 mm h⁻¹ and at an incidence angle of 78° the rain rate was 38 mm h⁻¹ (note that the latter dataset was obtained during a later experiment when a lower noise floor due to a hardware improvement was achieved).

At VV polarization, at all incidence angles, the radar Doppler spectra show two Doppler-shifted maxima. These Doppler shifts increase with incidence angle from ±7.5 Hz at 29° to ±9.7 Hz at 40°, ±12 Hz at 55°, and ±14.8 Hz at 78°, while the intensity of the backscattered radar power decreases. The radar Doppler spectra at HH polarization, 29° incidence angle, are similar to those at VV polarization. With increasing incidence angle (40°) the relative PSD at HH polarization decreases and a third, non-Doppler-shifted maximum occurs between the two maxima. At 55° incidence angle the non-Doppler-shifted maximum dominates over the two

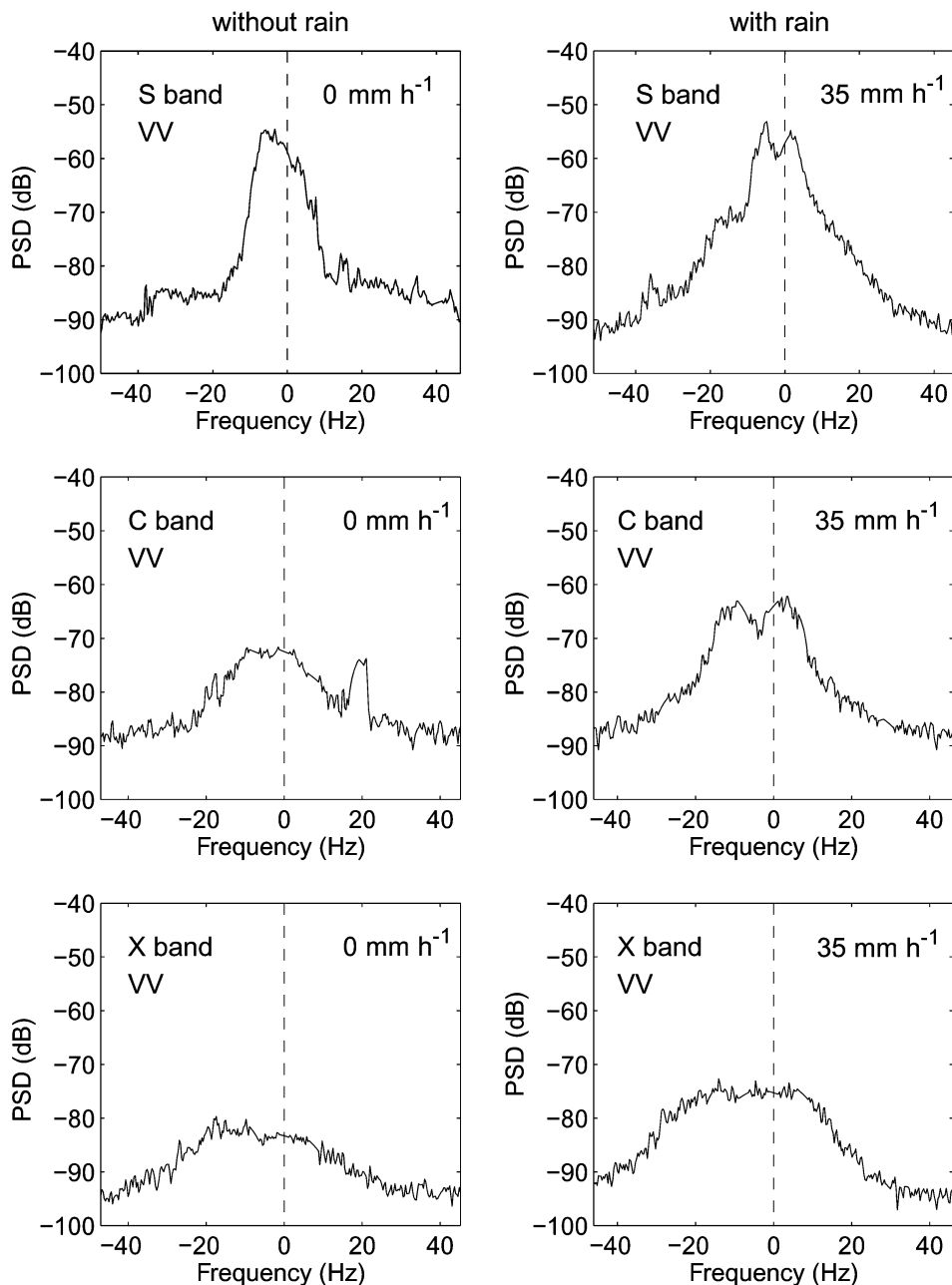


Figure 4. Radar Doppler spectra at VV polarization, different radar frequencies, and an incidence angle of 35° , field measurements. Left column: without rain (wind speed: 7.5 m s^{-1} , azimuth angle: 255°). Right column: with rain (wind speed: 6.5 m s^{-1} , azimuth angle: 275°). The time between the data acquisition (without rain/with rain) is 34 min.

Doppler-shifted maxima, and at 78° incidence angle only a single, non Doppler-shifted maximum was measured.

The spectral maximum of a pure ring-wave power spectrum for a drop diameter of 2.8 mm is at about 5–6 Hz (Bliven *et al.* 1997). At VV polarization at all measured

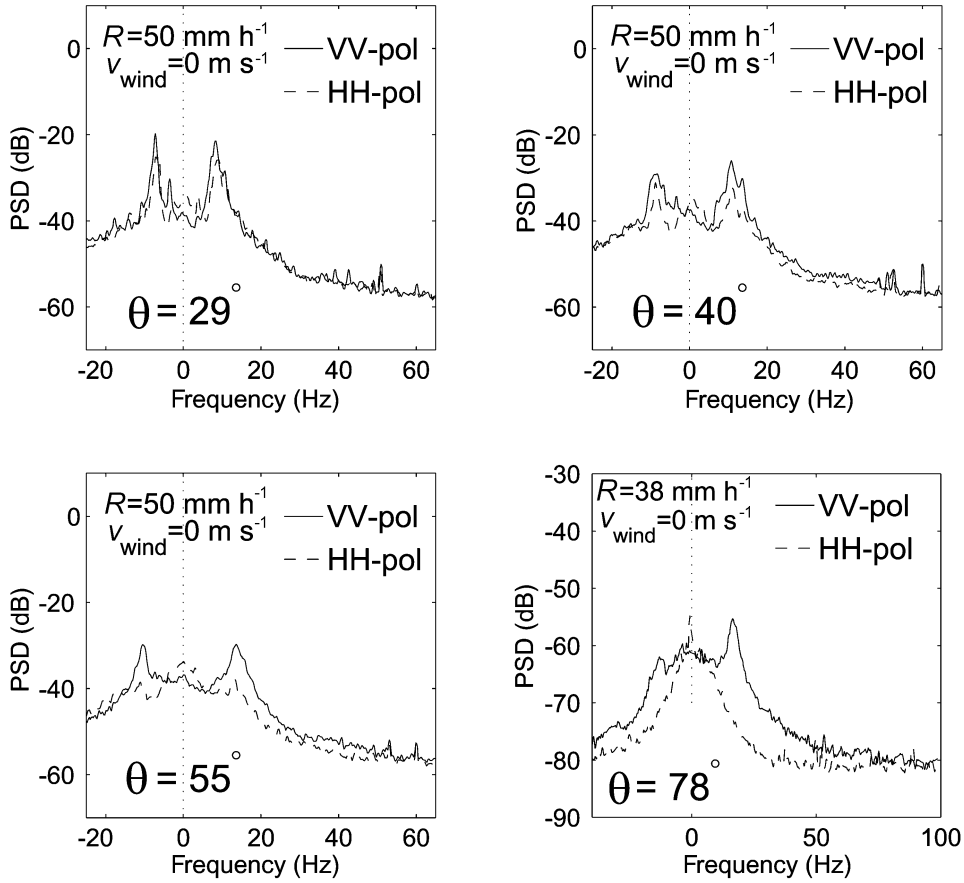


Figure 5. X band laboratory measurements of radar Doppler spectra at VV polarization (solid line) and HH polarization (dashed line) for different incidence angles at a fixed rain rate of 50 mm h⁻¹ (78°: 38 mm h⁻¹) without wind (note the different scales and lower noise floor at 78°).

incidence angles and radar frequencies, the two spectral maxima have Doppler frequencies corresponding to the ring waves' spectral maxima. Thus, Bragg scattering from ring waves is the dominant backscattering mechanism at VV polarization for all deployed incidence angles.

At HH polarization the radar backscatter at steep incidence angles is also caused by Bragg scattering at ring waves. With increasing incidence angle, however, the radar backscatter from rain-generated ring waves decreases and the radar backscatter from splash products which do not propagate increases. The strong zero Doppler-shifted maximum measured at high incidence angles implies that non-propagating features like stalks (Hansen 1986) are responsible for the radar backscattering. This is in accordance with radar backscatter calculations for grazing incidence angle by Wetzel (1990) and Craeye (1998).

3.3 Cross-polarization, field measurements

Figure 6 shows a strong rain-induced enhancement of the PSD for the same wind conditions as described for figure 4, but at C band, HV polarization. Due to the

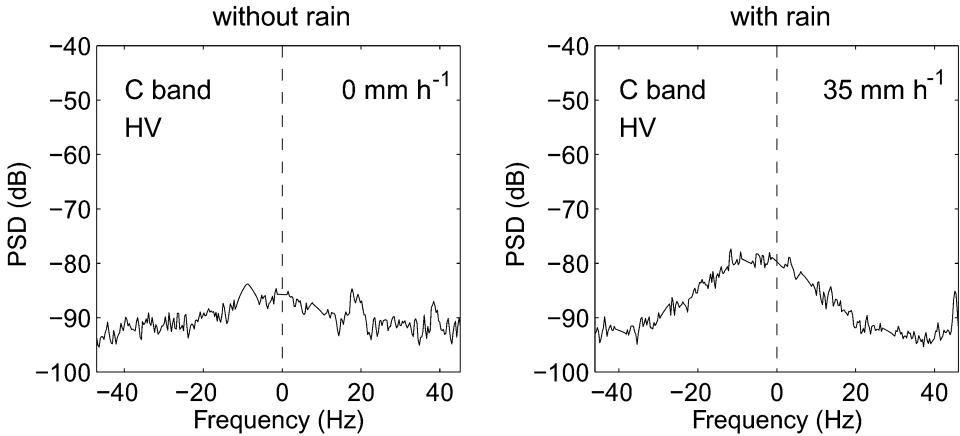


Figure 6. Same as figure 4 but only C band, HV polarization (incidence angle 35°).

action of rain, a broad maximum develops that shows only a slight overall Doppler shift caused by a weak current at ebb tide. The spike observed at C band (left panel) is due to electronic noise and was not considered in our analyses. This observation of rain under natural conditions is in accordance with former laboratory observations by Braun *et al.* (2002), who observed a rain-rate dependent enhancement of the X band radar backscattering at HV polarization. This enhancement was also observed at high wind speeds.

From the radar Doppler spectra's first moment at HV polarization the surface currents can be delineated (Braun 2003). This is possible even at higher wind speeds where the calculation of the surface drift from the overall shift of the two ring-wave maxima as suggested by Plant *et al.* (2003) is biased: at wind speeds higher than 5 m s^{-1} (measured in the wind-wave tank, see figure 6 in Braun *et al.* (2002)), the wind-wave maximum superimposes the ring-wave maxima, thus making current measurements difficult.

3.4 Wavenumber domains of wave damping and production

The ratios of the relative radar cross-sections for rain and wind (σ_{rw}) and wind only (σ_w) at VV polarization are shown in figure 7. In the encountered wind speed range ($4.5\text{--}17 \text{ m s}^{-1}$) and azimuth angle range ($155^\circ\text{--}305^\circ$) we did not observe any dependency of this ratio on wind speed and azimuth angle.

At S band (squares) the radar backscatter is reduced, at C band (circles) both a reduction and an enhancement occurs, and at X band (crosses) the radar backscatter is enhanced. The solid line denotes a linear regression to the data, and the dotted lines denote the limits of the 95% confidence interval of this regression. The transition wavenumber between wave damping and wave generation is about 100 rad m^{-1} , which corresponds to a Bragg wave frequency of 5.2 Hz and a wavelength of 6.3 cm (see point of intersection between the solid and dashed line). The herein encountered rain rates were up to 12 mm h^{-1} . Applying the same kind of analysis, Melsheimer *et al.* (1998) found a transition wavenumber of 63 rad m^{-1} , which corresponds to a wave frequency of 4 Hz and wavelength of 10 cm .

Former wind-wave tank experiments yielded a transition frequency of about 5 Hz calculated from wave amplitude spectra (of encounter) (Braun *et al.* 2002).

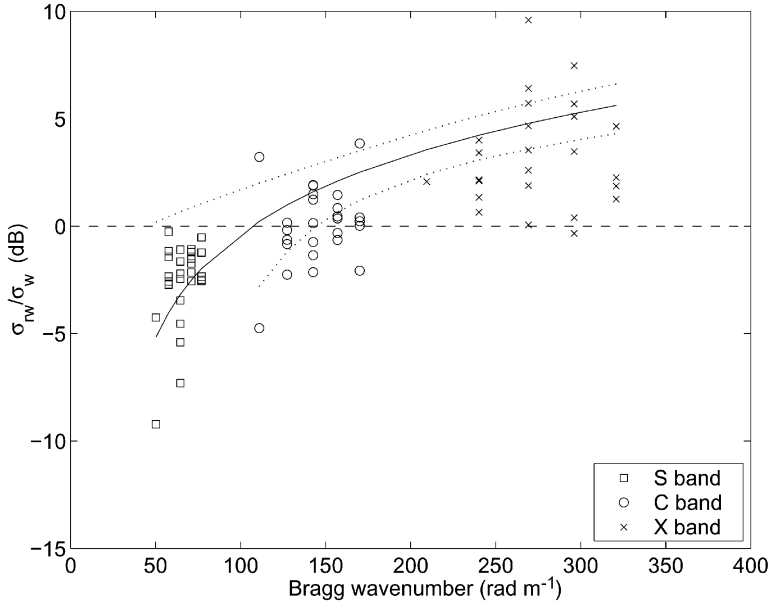


Figure 7. Ratio of the relative radar cross-sections at VV polarization at wind plus rain (σ_{rw}) and wind only (σ_w).

Contreras *et al.* (2003) conducted field measurements with a Ku band scatterometer. The Bragg wavenumber range of their transition region is between 200 and 300 rad m^{-1} (wave frequency 8.1–11.1 Hz, wavelength 2.1–3.1 cm). They mention that only few data show statistically significant decreases at low incidence angles (smaller wavenumbers), while the enhancement of the measured normalized radar cross-section was significant at higher incidence angles (larger wavenumbers).

During our field measurements, different rain rates were encountered, thus leading to different results. With increasing rain rate the maximum of the drop-size distribution is shifted towards larger drop sizes (Marshall and Palmer 1948, Willis and Tattelman 1989). An increasing drop size in turn causes a decreasing frequency of the spectral peak of the rain-induced ring waves (Houk and Green 1976, Lemaire *et al.* 2002). Thus, we hypothesize that the transition wavenumber is shifted towards lower wavenumbers with increasing rain rate, due to the increasing number of large drops in the drop-size distribution. We note that we could not observe this effect during our measurements because of the small number of samples and the lack of information on the drop-size distribution. The intensity of wave damping and roughness enhancement is affected by increasing wind speeds (Braun *et al.* 2002), but can still be observable even under strong wind conditions as images of rain bands in hurricanes show (Katsaros *et al.* 2000). Nevertheless, future measurements of the transition wavenumber should not only focus on the rain rate but also on the drop-size distribution to allow for an analytical determination of the transition wavenumber.

3.5 Estimating rain rates from radar cross-section ratios

The ratios of the relative radar cross-sections at S band, VV polarization and X band, VV polarization (hereinafter called SVV/XVV ratios) are reduced with

increasing wind speeds (without rain). This is in accordance with model calculations of Romeiser *et al.* (1997). Rain impinging on the water surface reduces this ratio by reducing the radar backscatter at S band and enhancing the radar backscatter at X band. Figure 8(a) shows the decrease of the SVV/XVV ratio due to the onset of rain with an averaged rain rate of about 4 mm h^{-1} during the measurement. The surface roughness is enhanced by impinging rain drops and σ_{rel} at X band increases. Due to the damping of the longer centimetre-scale waves, σ_{rel} at S band decreases. This can clearly be seen at time interval 4 (for each time step the radar cross-section is averaged over 30 s). Figure 8(b) shows the increase of the SVV/XVV ratio after the rain (averaged rain rate of about 6 mm h^{-1}) has stopped.

Comparing the SVV/XVV ratios for each dataset with constant wind conditions we set a flag where the SVV/XVV ratio was reduced due to rain by more than 3 dB (which we found to be a suitable value for this dataset with an rms. error of about $\pm 1 \text{ dB}$). Thus we were able to classify our data into classes of detected rain/no detected rain. With increasing rain rate and decreasing wind speed, the reduction of the SVV/XVV ratios increases. The minimum rain rate allowing a detection of rain was 2 mm h^{-1} . We did not observe any significant dependence of the SVV/XVV ratios on incidence angle and azimuth angle (in the range encountered during our experiments). With the antenna facing upwind we would expect this minimum rain rate to be higher because of the smaller enhancement of the radar backscatter at X band, as shown by Braun *et al.* (2002) who observed a saturation of the radar backscatter at high wind speeds. Therefore, we conclude that tower-based

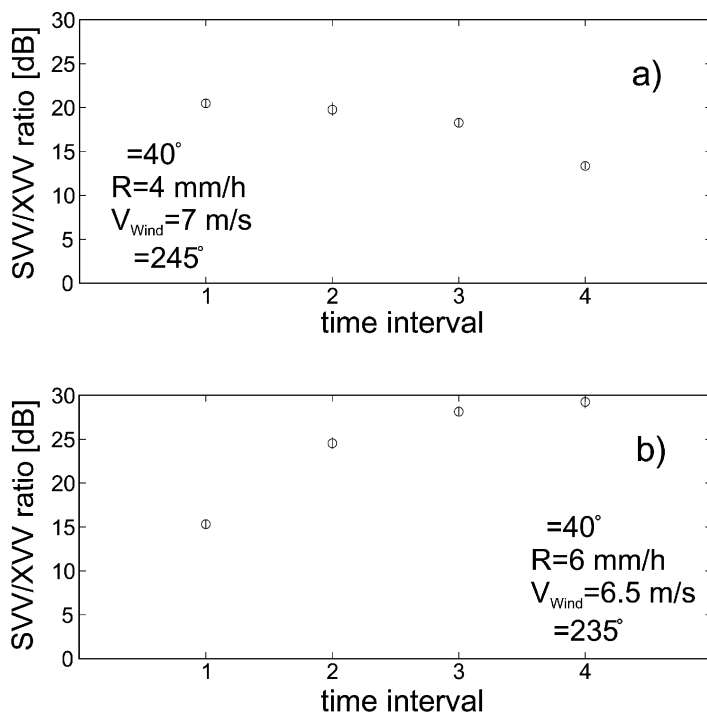


Figure 8. The circles denote the ratios of the relative radar cross-sections at S band, VV polarization and X band, VV polarization (SVV/XVV ratio). The lines inside the circles are error bars (average over 32 s). (a) shows the decrease of the SVV/XVV ratio due to the onset of rain while (b) shows the increase of the SVV/XVV ratio after the rain has stopped.

measurements of the SVV/XVV ratio with no atmospheric effects influencing the measured X band backscattered radar power (Melsheimer *et al.* 1998) can be used to detect rain. Further measurements with upwind/downwind/crosswind facing antennas are necessary to obtain a larger dataset and to consider drop-size distributions and, thus, to allow determination of rain rates by this approach.

The enhancement of the radar cross-section at C band, HV polarization in SIR-C/X-SAR data by rain was observed by Melsheimer *et al.* (1998), and its potential to estimate rain rates was discussed by Braun *et al.* (2002). During our measurements, we also observed a rain-induced enhancement of the radar backscatter at C band, HV polarization (however, the low signal-to-noise ratio allowed for calculating only few radar cross-sections). The observed reduction of the SVV/CHV ratio were up to 10 dB. Taking advantage of this effect we suggest a new method for estimating rain rates from multi-frequency/multi-polarization data. Since the radar backscatter at C band, cross-polarization is strongly enhanced in the presence of rain, and the radar backscatter at lower radar frequencies (S band or L band) is reduced, the SVV/CHV and/or LVV/CHV ratios may be suitable for providing estimates of rain rates. We are well aware that at present no multi-frequency/multi-polarization radar sensors are in operation that cover this frequency/polarization range. However, future satellite missions or sensors on different platforms with overlapping swaths may provide datasets that can be used in this respect.

As assumed by Melsheimer *et al.* (2001), and observed in our field measurements at S band, 35 mm h^{-1} rain, there may be cases where ring-wave generation can dominate wave damping and enhance the radar cross-section even at L band, if the drop-size distribution is shifted towards large drops. However, we assume that this is unlikely under similar conditions encountered during our field experiments with rain rates up to 12 mm h^{-1} .

4. Summary and conclusion

In order to gain better insight into the mechanisms responsible for signatures of rain events over the ocean on multi-frequency/multi-polarization SAR images, field and laboratory experiments were performed. During the field measurements, the backscattered radar power from the water surface was measured at different wind speeds, wind directions, and rain rates, as well as at different radar frequencies, polarizations, and incidence angles. During the laboratory measurements the backscattered radar power at X band was measured at different wind speeds and rain rates, as well as at different radar polarizations and incidence angles. Our field and laboratory results show that the dominant scattering mechanism of a rain-roughened water surface observed at all incidence angles at VV polarization is Bragg scattering from ring waves. At HH polarization the radar backscattering mechanism is dependent on incidence angle: at steep incidence angles Bragg scattering from ring waves occurs. With increasing incidence angle this effect diminishes and scattering from non-propagating splash products, like stalks, occurs.

The results from the field measurements show that the radar backscattering from the wind-roughened water surface is reduced at S band, and enhanced at X band while at C band a reduction or enhancement can occur. The enhancement and reduction of the sea-surface roughness by ring-waves and sub-surface phenomena, respectively, result in a transition wavenumber of about 100 rad m^{-1} (5.2 Hz). This result is in agreement with the results of previous laboratory investigations (Braun *et al.* 2002), where a transition frequency of encounter of about 5 Hz was measured,

as well as with observations of multi-frequency/multi-polarization SAR images performed by Melsheimer *et al.* (1998), who found a transition wavenumber of 63 rad m^{-1} (corresponding to a wave frequency of 4 Hz). We hypothesize that the transition wavenumber depends on the drop-size distribution of the rain.

Taking into consideration the different dependencies of the radar backscatter at different frequencies and polarizations on rain rate, we have suggested a method to estimate rain rates by calculating the ratio of the radar cross-sections at L band, VV polarization and at C band, HV polarization. Provided an availability of SAR data at the respective frequency/polarization combinations, this method will allow investigation of the nature of small-scale (convective) rain events over the ocean by analysing multi-frequency/multi-polarization SAR images. To validate this method, we suggest performing further field measurements with a scatterometer operating in L band, VV polarization and C band, HV polarization.

Acknowledgements

The authors would like to thank Philipp A. Lange and Sönke Heyen who helped in preparing the measurements at the wind-wave tank of the University of Hamburg, and Alexandra Bayer, Ute Hochbaum and Hanno von Knobloch, who helped in preparing the field measurements. The authors would also like to thank the department of RegDir. K. Schroh of the SBM (Sonderstelle des Bundes zur Bekämpfung von Meeresverschmutzungen) and H.-J. Hoppe from the WSA (Wasser- und Schifffahrtsamt Cuxhaven) for their support in performing the field measurements at the tower of the WSA. This work was funded by the Federal Ministry of Education, Research, Science, and Technology (BMBF) under contract 01 LA 9819/2 ('AURORA').

References

- ATLAS, D., 1994, Footprints of storm on the sea: a view from a spaceborne synthetic aperture radar. *Journal of Geophysical Research*, **99**, pp. 7961–7969.
- BLIVEN, L.F., BRANGER, H., SOBIESKI, P. and GIOVANANGELI, J.-R., 1993, An analysis of scatterometer returns from a water surface agitated by artificial rain: evidence that ring waves are the main feature. *International Journal of Remote Sensing*, **14**, pp. 2315–2329.
- BLIVEN, L.F., SOBIESKI, P.W. and CRAEYE, C., 1997, Rain generated ring-waves: measurements and modelling for remote sensing. *International Journal of Remote Sensing*, **18**, pp. 221–228.
- BRAUN, N., 2003, Untersuchungen zur Radar-Rückstreuung und Wellendämpfung beregneter Wasseroberflächen. Dissertation, Shaker Verlag, Aachen, Germany.
- BRAUN, N., GADE, M. and LANGE, P.A., 2002, The effect of artificial rain on wave spectra and multi-polarization X band radar backscatter. *International Journal of Remote Sensing*, **23**, pp. 4305–4323.
- CRAEYE, C., 1998, Radar signature of the sea surface perturbed by rain, PhD thesis, Université Catholique de Louvain, France.
- CONTRERAS, R.F., PLANT, W.J., KELLER, W.C., HAYES, K. and NYSTUEN, J., 2003, Effects of rain on Ku-band backscatter from the ocean. *Journal of Geophysical Research*, **108**, 3165, DOI 10.1029/2001JC001255.
- FU, L. and HOLT, B., 1982, Seasat views of the oceans and sea ice with synthetic aperture radar. JPL Publication 81–120, Jet Propulsion Laboratory, Pasadena, California, pp. 106–107.
- HANSEN, J.P., 1986, Rain backscatter tests dispel old theories. *Microwaves & RF Journal*, **6**, pp. 97–102.

- HOUK, D. and GREEN, T., 1976, A note on surface waves due to rain. *Journal of Geophysical Research*, **81**, pp. 4482–4484.
- HÜHNERFUß, H., LANGE, P.A., TEICHERT, J. and VOLLMERS, H., 1976, A wind wave tunnel for the investigation of artificial slick wave damping and drift. *Meerestechnik (Marine Technology)*, **7**, pp. 23–26.
- KATSAROS, K., VACHON, P.W., BLACK, P.G., DODGE, P.P. and UHLHORN, E.W., 2000, Wind fields from SAR: Could they improve our understanding of storm dynamics? *Johns Hopkins APL Technical Digest*, **21**, pp. 86–93.
- LEMAIRE, D., BLIVEN, L.F., CRAEYE, C. and SOBIESKI, P., 2002, Drop size effects on rain-generated ring-waves with a view to remote sensing applications. *International Journal of Remote Sensing*, **23**, pp. 2345–2357.
- MARSHALL, J.S. and PALMER, W.M.K., 1948, The distribution of raindrops with size. *Journal of Meteorology*, **5**, pp. 165–166.
- MELSHEIMER, C., ALPERS, W. and GADE, M., 1998, Investigation of multi-frequency/multi-polarization radar signatures of rain cells using SIR-C/X-SAR data. *Journal of Geophysical Research*, **103**, pp. 18867–18884.
- MELSHEIMER, C., ALPERS, W. and GADE, M., 2001, Simultaneous observations of rain cells over the ocean by the synthetic aperture radar aboard the ERS satellites and by surface-based weather radars. *Journal of Geophysical Research*, **106**, pp. 4665–4678.
- PLANT, W.J., KELLER, W.C., HAYES, K. and NYSTUEN, J., 2003, Rainfall and river currents retrieved from microwave backscatter. In *Proceedings of the IEEE International Geophysical Remote Sensing Symposium*, Toulouse, France.
- ROMEISER, R., ALPERS, W. and WISMANN, V., 1997, An improved composite surface model for the radar backscattering cross section of the ocean surface I. Theory of the model and optimization/validation by scatterometer data. *Journal of Geophysical Research*, **102**, pp. 25237–25250.
- WETZEL, L.B., 1990, On the theory of electromagnetic scattering from a raindrop splash. *Radio Science*, **25**, pp. 1183–1197.
- WILLIS, P.T. and TATTELMAN, P., 1989, Drop-size distributions associated with intense rainfall. *Journal of Applied Meteorology*, **28**, pp. 3–15.
- WISMANN, V., 1994, The 5-frequency multi-polarization scatterometer HELISCAT of the University of Hamburg for operation on a small helicopter. Technical Report, University of Hamburg, Hamburg, Germany.